CALCULATION OF YIELD SURFACES AND DETERMINATION OF FORMING LIMIT DIAGRAMS OF ALUMINIUM ALLOYS

J. J. FUNDENBERGER,† M. J. PHILIPPE,† C. ESLING,† P. LEQUEU‡
and B. CHENAL‡

† LM2P-ISGMP, Ile du Saulcy, F-57045 Metz Cedex 01
‡ CRV Pechiney-Centr'Alp, B.P. 27, F-38340 Voreppe

In order to point out the influence of the crystallographic texture on the formability of 2 aluminium alloys, the orientation distribution function (ODF) will be carried out using the series expansion method. Combining the ODF with a Taylor plastic deformation model we are able to calculate the yield loci and to predict the plastic strain ratio which is of high interest in the formability.

KEY WORDS Yield locus, forming limit diagram, ODF-calculation, aluminium alloy, anisotropy, strain hardening coefficient, plastic strain ratio, yield stress.

1. INTRODUCTION

The purpose of this contribution is to develop tools in order to predict and understand formability of aluminium alloy sheets. These tools are:

—the O.D.F. (orientation distribution function) calculated with ghost correction.

—the yield loci calculation including the anisotropy of the material in form of the O.D.F.

—the forming limit diagrams which allow a direct evaluation of the formability of a sheet.

The present work concerns 2 aluminium alloy sheets, for which we have made a study on their formability related to the crystallographic texture. We will first specify the experimental conditions, and after having exposed the results, we will discuss the relations between the different parameters.

2. EXPERIMENTAL PROCEDURES

2.1. *Materials*

The sheets were supplied by the Centre de Recherche de Voreppe of Pechiney. The chemical composition of both materials is given in Table 1.

The AlMgSi alloy referenced ASG 25 is an industrial alloy. It was hot rolled down to 4 mm thickness, the final thickness (1.3 mm) was obtained by cold

Table I Chemical composition of the studied alloys.

Alloy		Li	Cu	Mg	Zn	Fe	Si	Ti	Zr	Cr	Mn
Al Li	min	1.7	1.8	1.1	0.04	0.30	0.20	0.10	0.04		
	max	2.3	2.5	1.9	0.16				0.16		
Al Mg Si	min			0.30			1.00				
	max		0.20	0.65	0.10	0.40	1.40	0.10		0.05	0.15

rolling. The following heat treatments consist in a solution treatment and a quenching which gives the AlMgSi alloy its final properties.

The 2091 alloy is an AlLi alloy. It was hot rolled down to 3.7 mm and cold rolled down to 1.6 mm. It was then annealed for 1 hour at 415°C. This heat treatment does not correspond to the one used industrially for forming purposes.

2.2. *Microstructure*

Microstructural characterization was carried out using optical microscopy. The sample preparation consists in an electrolytical polishing and an electrolytical etching.

Microstructural examination using T.E.M. (Venkateswara *et al.*, 1989) r-evealed that the AlLi alloy is strengthened by δ' (Al_3Li) precipitates and β' (Al_3Zr) dispersoïds.

The AlMgSi alloy is strengthened by fine homogeneous distribution of Mg_2Si precipitates. When combining in Mg_2Si precipitates, the Mg/Si mass ratio is equal to 1.73. In the AlMgSi alloy this Mg/Si ratio is equal to 0.40, Si is then in excess, hence leading to an improvement of the mechanical properties, but also to a decrease of the corrosion resistance.

2.3. *Texture*

For each sample the (111), (200) and (220) pole figures were measured by X-ray diffraction with a texture goniometer. The three dimensional crystallite orientation distribution functions (O.D.F.) were calculated using the series expansion method (Bunge, 1969). In this method the O.D.F. is expressed by series of generalized spherical harmonics. Including the positivity of the pole figures and of the O.D.F. in this method, we obtain a set of coefficients which describe the texture:

$$f(g) = \sum_l \sum_m \sum_n C_l^{mn} T_l^{mn}(g) \tag{1}$$

By means of these coefficients, the computation of complete pole figures as well as sections of the ODF in the Euler space is straightforward. The software used for texture analysis has been developed at the LM2P laboratory.

In order to improve the measurements in the case of the AlMgSi alloy, the large grain size leads us to perform several measurements through the thickness of the sheet. Thus the pole figures which were used for the texture analysis are in fact obtained by superimposing the pole figures measured at the surface, at the 3/4, at the 1/2 and at the 1/4 of the thickness.

2.4. *Mechanical Properties*

The mechanical properties were determined using tensile tests at room temperature and constant displacement rate. The strain hardening coefficient corresponds to the Hollomon law:

$$\sigma = k\varepsilon^n \tag{2}$$

The plastic strain ratio was continuously measured during the tensile test. The mean value was calculated by:

$$\bar{r} = \frac{r_0 + 2r_{45} + r_{90}}{4} \tag{3}$$

and:

$$\Delta r = \frac{r_0 - 2r_{45} + r_{90}}{2} \tag{4}$$

2.5. *The Yield Loci*

The yield loci were computed in the framework of a Taylor–Bishop–Hill theory. The software was provided by P. Van Houtte, from Katholieke Universiteit Leuven. The method has already been described in detail by several authors (Bunge *et al.*, 1970, Bunge *et al.*, 1980; Mols *et al.*, 1984, Van Houtte, 1987, 1989). We will just give a short recalling of this method. If we assume that the Taylor factor $M(g, q)$ could be developed in a series expansion on generalized spherical harmonics, we can write:

$$M(g, q) = \sum_l \sum_m \sum_n m_l^{mn}(q) T_l^{mn}(g) \tag{5}$$

the average Taylor factor over the polycrystal is:

$$\bar{M}(q) = \oint_g M(g, q) f(g)\, dg \tag{6}$$

using the series expansion of the ODF and of the Taylor factor:

$$\bar{M}(q) = \sum_l \sum_m \sum_n \frac{m_l^{mn}(q) C_l^{mn}}{2l + 1} \tag{7}$$

The plastic work rate can be expressed as a function of the average Taylor factor:

$$\overset{\star}{W} = \tau_c E_{eq}(q) \bar{M}(q) \tag{8}$$

where τ_c denotes the critical resolved shear stress, and $E_{eq}(q)$ the equivalent strain rate.

The average work rate is also given by another expression:

$$\overset{\star}{W} = E_{ij}(q) \sigma_{ij} \tag{9}$$

where σ_{ij} denotes the components of the deviatoric stress tensor, thus it follows:

$$E_{ij}(q)\sigma_{ij} = \tau_c E_{eq}(q) \bar{M}(q) \tag{10}$$

This relation allows to calculate the stress for a given strain mode using the average Taylor factor. A scanning of all the strain modes leads to a complete yield locus in a 5 dimensional space. For convenience reasons one plots 2 dimensional sections of the yield locus. In order to build the 2 dimensional sections, we are looking for the yield stress σ_y for a given direction **U** in stress space. By choosing the direction **U** we select the section to be determined (Van Houtte, 1987; Van Houtte *et al.*, 1989).

The calculation of the $r(\alpha)$ value is based on the following reasoning: for a given α angle between the sample axis and the R.D. we assume that the true value of q corresponds to a minimum of the required deformation work, i.e. to the minimum of the Taylor factor. When finding this minimum and the corresponding q_{min} value, the plastic strain ratio is given by:

$$r(\alpha) = \frac{q_{min}(\alpha)}{1 - q_{min}(\alpha)} \tag{11}$$

Aluminium is an fcc metal, the slip systems used in the computations belong to the $(111)\langle 110 \rangle$ family.

2.6. *The Forming Limit Diagrams*

The forming limit diagrams were determined in direct deformation mode. Drawing ($\varepsilon_1 > 0$, $\varepsilon_2 < 0$) is simulated by uniaxial tensile tests. Plane strain ($\varepsilon_1 > 0$, $\varepsilon_2 = 0$) is simulated by tensile tests on notched tensile samples. Expansion ($\varepsilon_1 > 0$, $\varepsilon_2 > 0$) is achieved by a bulge test. The grid used for measuring the deformations is composed of secant circles with a 2 mm diameter. The deformation measurements were performed by means of an episcope with a magnification of 20. The deformation at necking were determined using Bragard method (Parnière and Sanz, 1976).

3. RESULTS

3.1. *Microstructure*

The grain size of the AlMgSi alloy was rather homogeneous in the order of 50 μm. The grains were slightly elongated in the rolling direction. The grain size of the AlLi alloy was inhomogeneous, bands of large elongated, partially recrystallised grains (70 μm) can be found in a very fine grain (3 μm) structure. This microstructure is due to the non industrial annealing conditions.

3.2. *The texture*

The pole figures presented in Figures 1 and 2 were recalculated from the C_l^{mn} coefficients of the series expansion Eq. (1).

For the AlLi sheet, the maximum of the ODF approaches the value of 14.20 in multiples of random, the texture is very sharp (see Figure 3). For the main orientation, the $\langle 211 \rangle$ direction lies in R.D.

The texture of the AlMgSi sheet is weaker, with a maximum of 7.35 in multiples of random (see Figure 4). The main orientation is the $(001)\langle 100 \rangle$
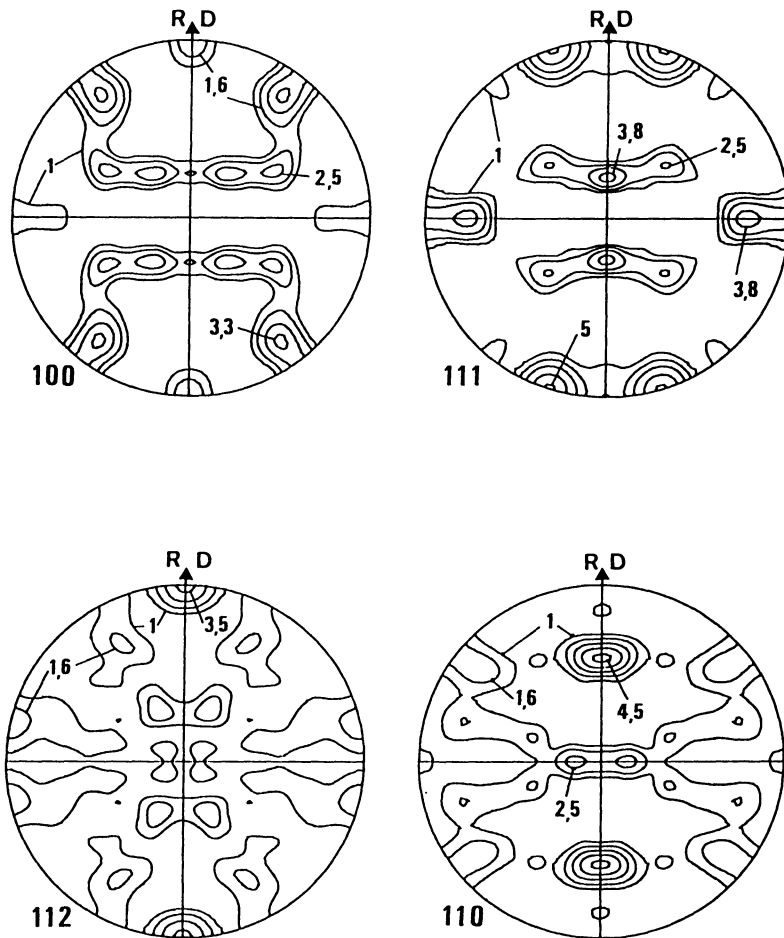
Figure 1 Pole figures of the AlLi alloy.

orientation, known as the cube orientation. The texture shows also secondary orientations which are quite strong.

The textures of these 2 materials are different. One can expect that the polycrystal properties will reflect these differences too.

3.3. *Mechanical properties*

3.3.1. *Tensile test.* The results of the tensile tests are given in Table 2 and 3. In the case of the AlLi alloy, the yield strength and the maximum stress are high and show large variations with the angle α of the test axis to RD. The maximum elongation is quite low (15%). The shape of the stress strain curves are typically of Portevin–Le Chatelier effect (see Figure 5).

The AlMgSi alloy has a more or less constant yield strength and maximum stress with respect to the cutting angle. The maximum elongations approach 30%. The stress–strain curves are smooth (see Figure 5).
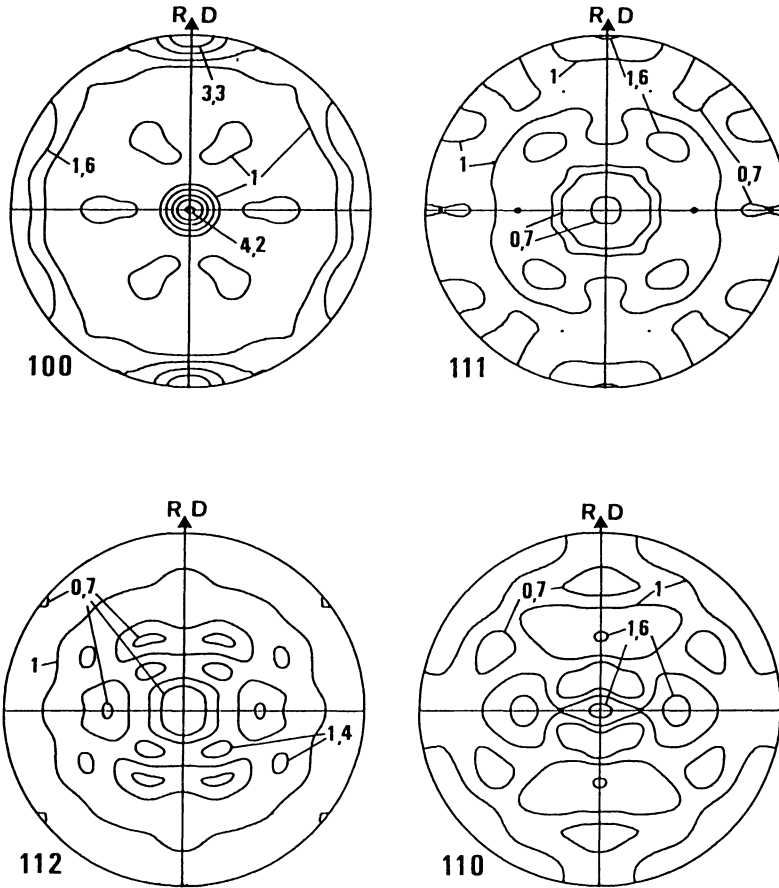
Figure 2   Pole figures of the AlMgSi alloy.

3.3.2. The strain hardening coefficient. The variations of the strain hardening coefficient in the sheet plane are weak regarding the AlMgSi alloy (see Figure 6), its mean value is about 0.265. The variations are important in AlLi alloy, with a maximum (0.216) at 45° from the R.D., but the values of the strain hardening coefficient are always low. In the case of the AlLi alloy the values of the strain hardening coefficient must be considered as unconfirmed, because the stress–strain curves presents much discontinuities due to the Portevin-Le Chatelier effect.

3.3.3. The plastic strain ratio. The plastic strain ratio of the AlMgSi alloy shows little variations with the α angle ($r = 0.548$, $\Delta r = 0.156$). The calculated values show the same variations and they are close to the measured ones (see Figure 7).

The plastic strain ratio of the AlLi alloy shows large variations with the α angle, the maximum is located at 50° from R.D. ($r = 1.016$, $\Delta r = 1.795$). The comparison with the calculated values is quite good. Nevertheless, the calculated variations are somewhat higher than the measured ones (see Figure 8).
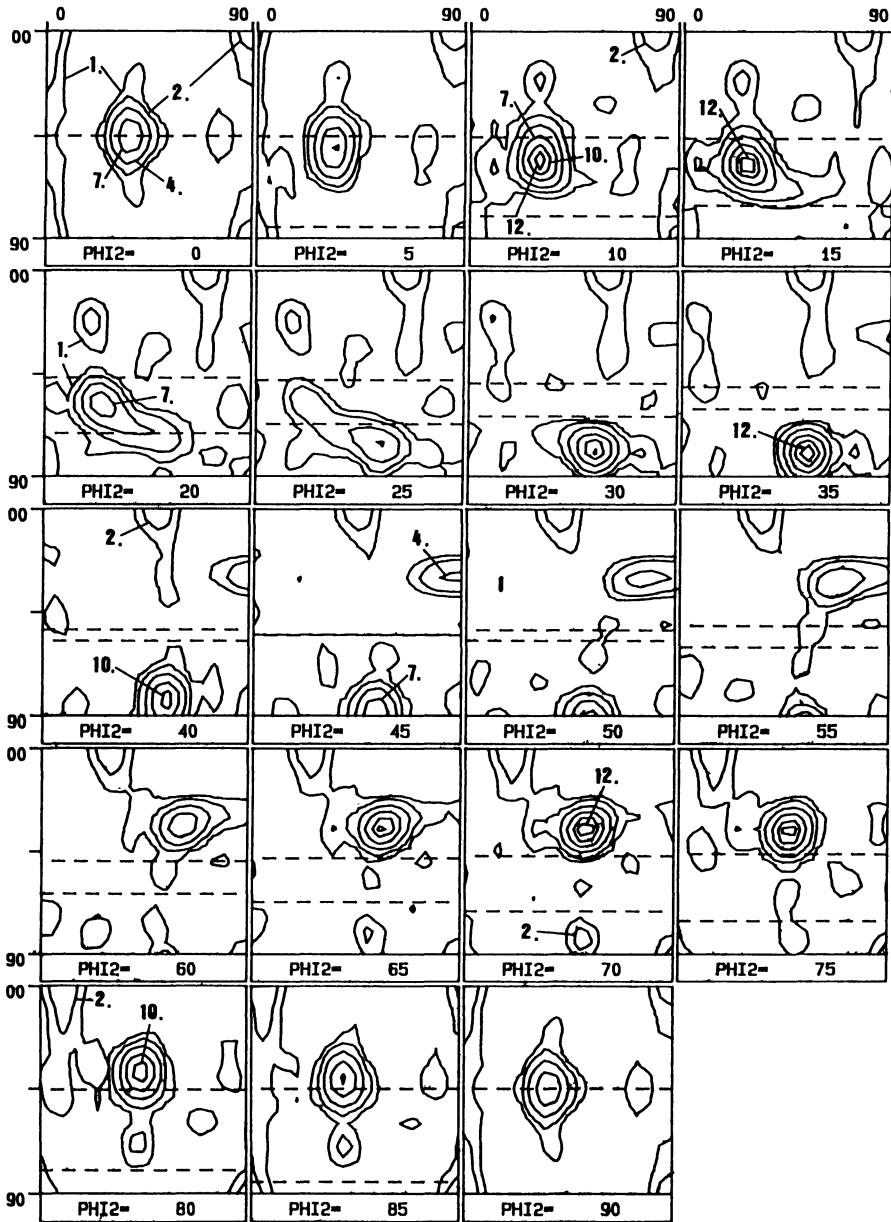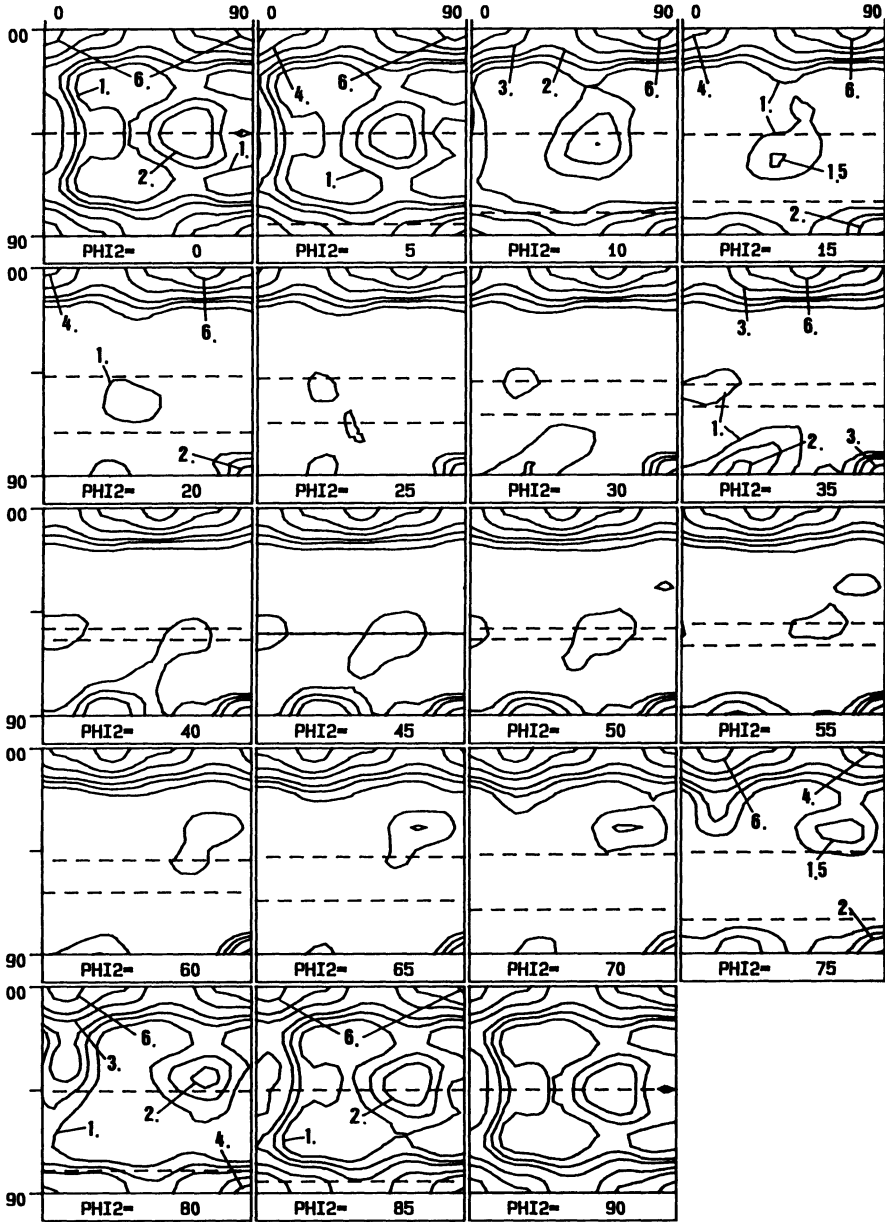
Figure 3 O.D.F. sections of the AlLi alloy.

J. J. FUNDENBERGER *ET AL.*

Figure 4   O.D.F. section of the AlMgSi alloy.

Table 2 Results of the tensile tests: AlLi alloy

Angle	n	r at 10%	calculated	Yield str. MPa	max str. MPa	% elongation
0°	0.172	0.50	0.96	154	260	13.5
0°	0.191	0.50		155	259	14.4
15°	0.192	0.50	0.86	148	254	13.4
15°	0.205	0.45		150	254	11.8
30°	0.197	1.05	1.47	147	252	13.9
30°	0.189	1.11		147	252	14.3
45°	0.219	1.86	2.91	149	240	21.6
45°	0.213	2.13		147	238	17.7
60°	0.191	1.74	2.48	152	241	24.9
60°	0.196	1.95		152	242	22.7
75°	0.198	0.40	1.00	157	260	20.3
75°	0.195	0.30		159	260	16.5
90°	0.198		0.75	159	267	16.1
90°	0.198	0.20		161	270	16.5
		$\bar{r} = 1.17$	$\bar{r} = 1.89$			
		$\Delta r = 1.65$	$\Delta r = 2.07$			

We can also point out that the calculation only takes the texture into account, and not other structural parameters. Microstructural anisotropy effects such as microbands and dense dislocation walls have also an influence on the flow stress anisotropy (Juul Jensen and Hansen, 1990).

3.3.4. *The yield loci.* The yield loci are quite similar for both alloys (see Figures 10 and 11). The experimental yield locus determination needs a large number of time consuming tests. Therefore we restrict our investigations to the yield stress $\sigma_y(\alpha)$ measured every 15° according to R.D. The calculated curves are adjusted using the value of the yield stress $\sigma_y(\alpha)$ in the R.D. as a reference.

**Table 3** Results of the tensile tests: AlMgSi alloy.

| Angle	n	r at 10%	calculated	Yield str. MPa	max str. MPa	% elongation
0°	0.260	0.610	0.61	114	233	29.2
0°	0.263	0.624		113	233	26.5
15°	0.269	0.547	0.57	113	232	24.0
15°	0.269	0.559		112	233	31.7
30°	0.272	0.497	0.51	112	231	30.6
30°	0.272	0.494		111	231	26.1
45°	0.271	0.472	0.47	111	231	25.6
45°	0.271	0.483		112	230	28.1
60°	0.266		0.49	113	231	28.6
60°	0.268			112	231	28.6
75°	0.267	0.590	0.58	113	230	24.9
75°	0.267	0.584		111	230	31.7
90°	0.267	0.638	0.61	111	229	26.1
90°	0.266	0.629		112	230	30.3
		$\bar{r} = 0.55$	$\bar{r} = 0.54$			
		$\Delta r = 0.15$	$\Delta r = 0.14$			
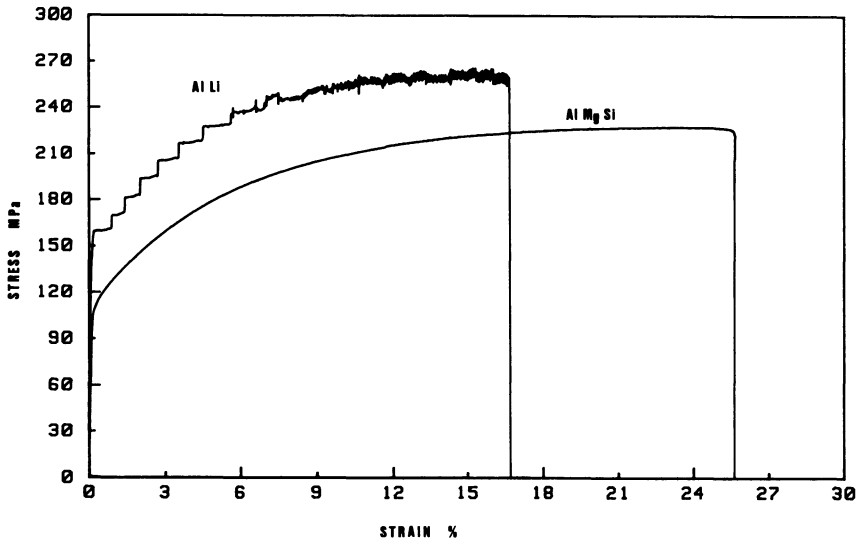
Figure 5   Stress–strain curves: Portevin–Le Chatelier effect.

Concerning the AlLi alloy, there are but small differences between the calculations and the measurements (see Figure 12). The calculations reproduce well the observed experimental variations.

For the AlMgSi alloy, the calculated and the measured values are more or less constant (see Figure 13). The differences visible in the Figure 13 are exaggerated by the scale of the plot. The relative differences are weak in both cases: lower than 5.5% for the AlMgSi alloy and lower than 2.2% for the AlLi alloy.
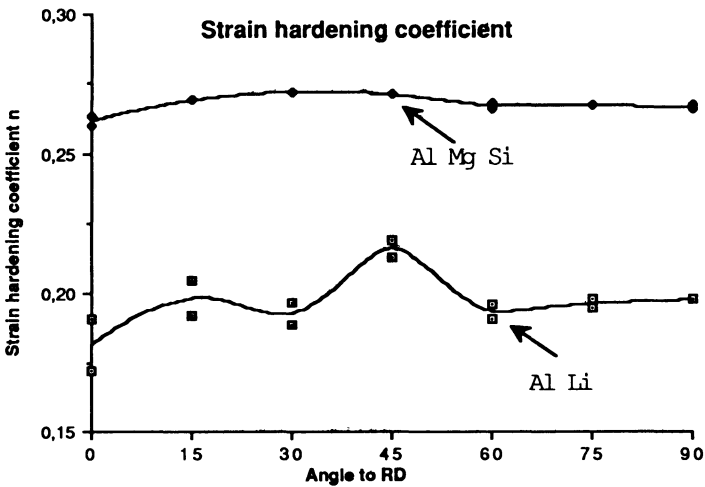
Figure 6   Strain hardening coefficient versus the cutting angle with respect to RD. Comparison of the two alloys.
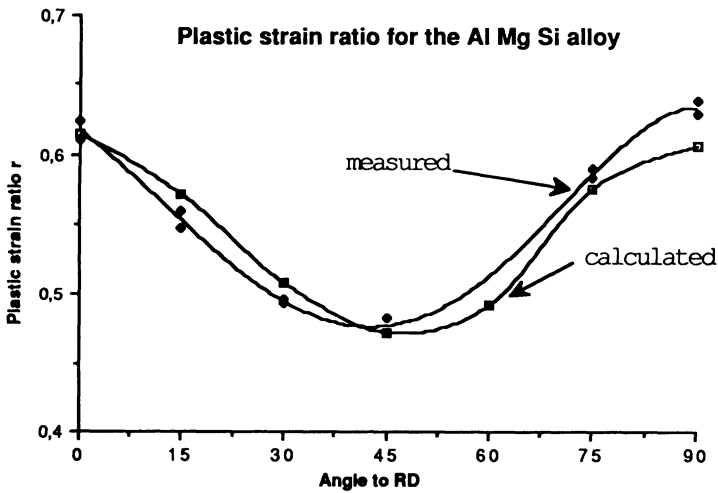
Figure 7 Plastic strain ratio versus the cutting angle with respect to RD. Comparison of measurement and prediction.

3.3.5. *The forming limit diagrams.* The forming limit diagrams were plotted at fracture and at necking (see Figures 14 and 15). The deformations in plane strain are underestimated due to the strong deformation gradient existing in the notched samples. Especially for necking because we use the Bragard method which takes into account a quite large area around the fracture. The AlMgSi alloy shows a better formability in expansion as well as in drawing. This is in agreement with the values of the plastic strain ratio and the hardening coefficient which are of high interest to predict the shape of the FLD. The AlMgSi alloy has the highest
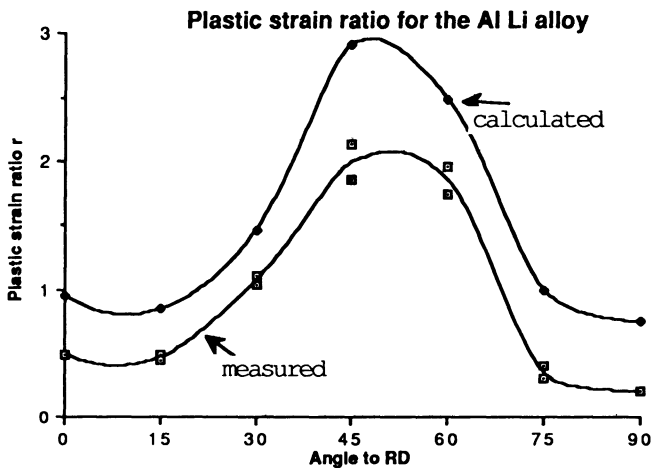
Figure 8 Plastic strain ratio versus the cutting angle with respect to RD. Comparison of measurement and prediction.
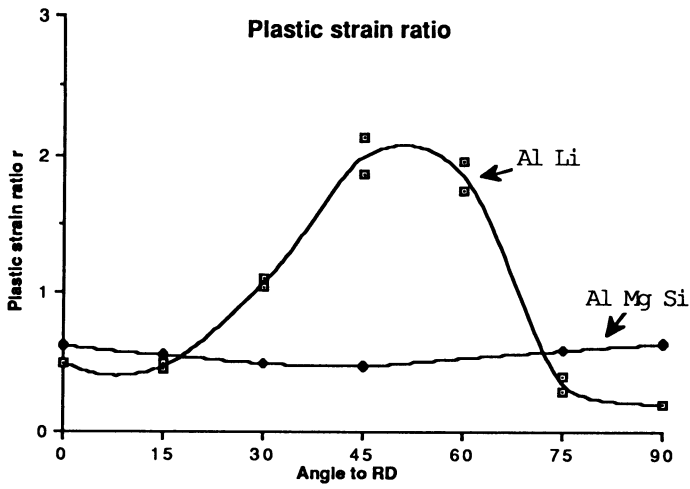
Figure 9 Plastic strain ratio versus the cutting angle with respect to RD. Comparison of the two alloys.
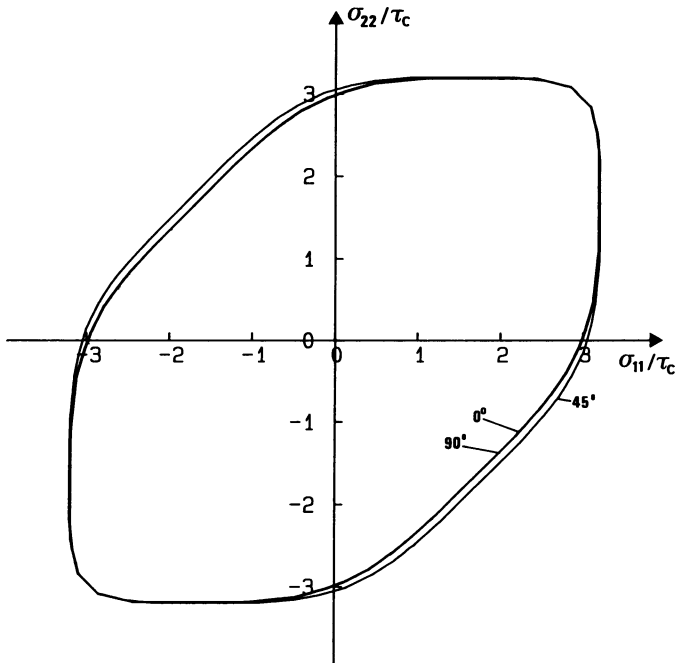
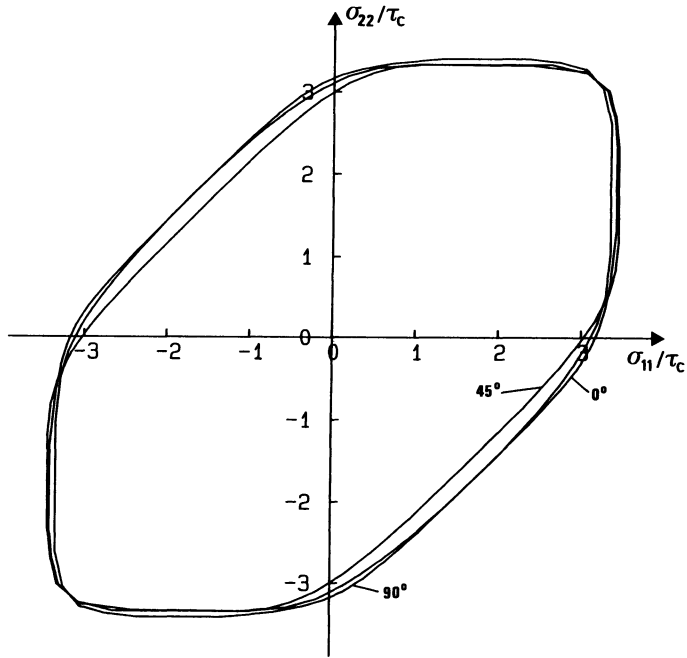**Figure 10** Calculated yield loci for the AlMgSi alloy. (Cutting angles 0°, 45°, 90°).

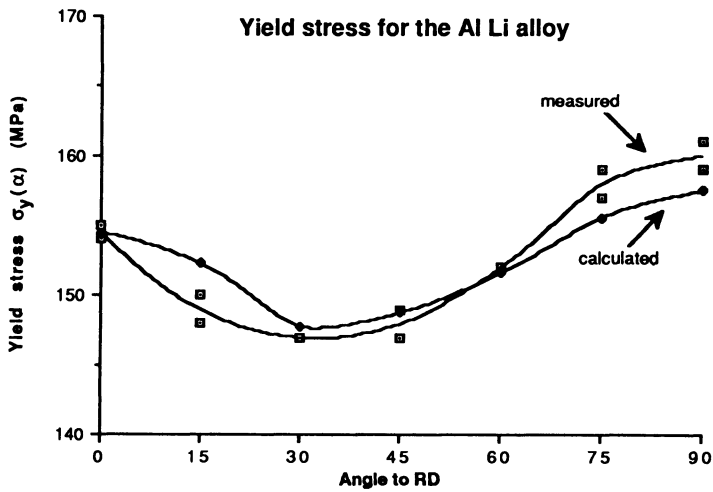**Figure 11** Calculated yield loci for the AlLi alloy. (Cutting angles 0°, 45°, 90°).

Figure 12 Yield strength versus the cutting angle with respect to RD. Comparison of the measurement and the prediction.
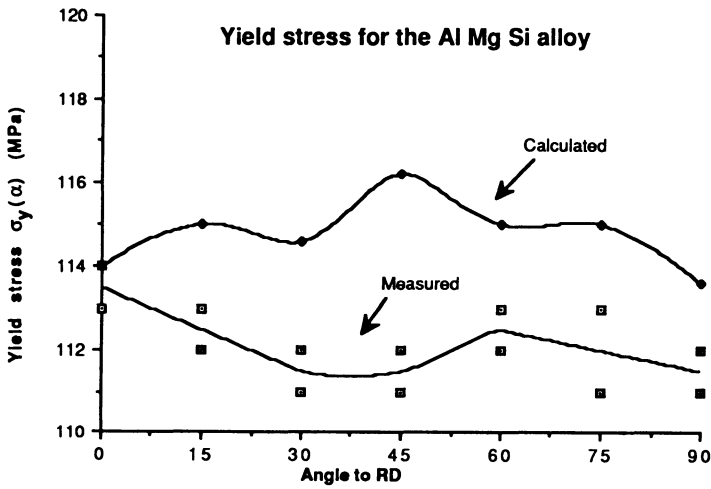
Figure 13 Yield strength versus the cutting angle with respect to RD. Comparison of the measurement and the prediction.

hardening coefficient, which increases the level of the deformations in the FLD and at the same time, the curve becomes flatter in the expansion field.

The plastic strain ratio has been defined by:

$$r = \frac{\varepsilon_2}{\varepsilon_3} \tag{12}$$

The volume remaining constant during plastic deformation:

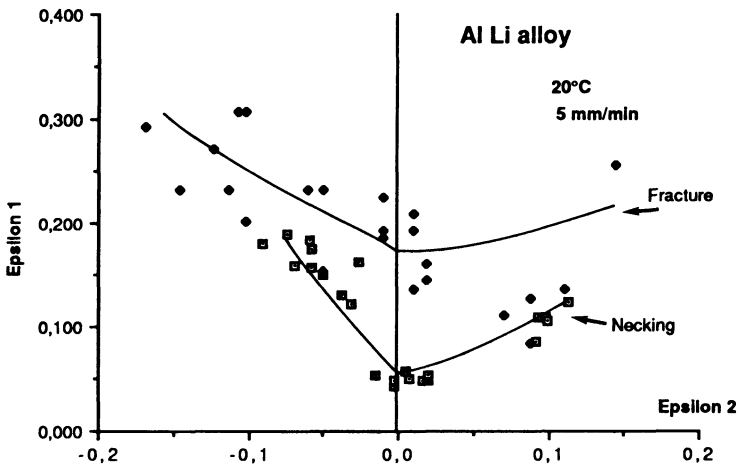$$r = \frac{-\varepsilon_2}{\varepsilon_1 + \varepsilon_2} \tag{13}$$

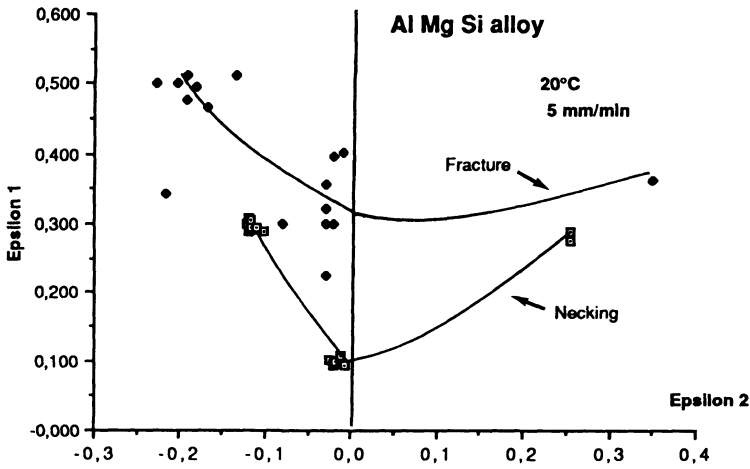**Figure 14** Forming limit diagrams of the AlLi alloy.

Figure 15 Forming limit diagrams of the AlMgSi alloy.

hence:

$$\varepsilon_1 = \frac{-(r+1)}{r}\varepsilon_2 \tag{14}$$

the limit of the FLD in drawing is then related to the value of the anisotropy ratio. When the r value is high, the deformation in drawing increases. But the Δr value plays also an important role. For the AlMgSi alloy, both the r and Δr value are lower than those for the AlLi alloy. We can see that the formability of AlMgSi is better than for AlLi, which is certainly due to the smaller Δr value.

4. CONCLUSION

The strong texture of the AlLi alloy leads to a strong planar anisotropy (see curves $r(\alpha)$, $n(\alpha)$ and $\sigma_y(\alpha)$). The microstructure and the chemical composition confers to this alloy a high mechanical strength. The metallurgical state of the AlLi alloy resulted from a heat treatment which does not correspond to the one used industrially for forming purposes. This may explain the formability which is low, according to the structural parameters and the $r(\alpha)$ and $n(\alpha)$ values. The texture of the AlMgSi alloy had a main component $(001)\langle 100 \rangle$ but also strong secondary orientations. This texture leads to a small anisotropy (see curves $r(\alpha)$, $n(\alpha)$ and $\sigma_y(\alpha)$). The formability of this alloy is good according to the $r(\alpha)$ and $n(\alpha)$ values. The obtained results underline the importance of the crystallographic texture in the formability.

References

Bunge, H. J. (1969). Mathematische Methoden der Texturanalyse, Akademie-Verlag (Berlin).
Bunge, H. J. (1970). Some applications of the Taylor theory of polycrystal plasticity, Krisstal Tecn., No. 5, 145–175.

Bunge, H. J., Schulze, M. and Grzesik, D. (1980). Calculation of the Yield Locus of polycrystalline materials according to the Taylor theory, Peine Salzgitter, p. 1–31.

Jalinier, J. M. (1981). Mise en forme et endommagement, Thèse de Doctorat d'Etat.

Juul Jensen, D. and Hansen, N. (1990). Flow stress anisotropy in aluminium. *Acta Met.* **38,** 8, 1369–1380.

Mols, K., Van Praet, K. and Van Houtte, P. (1984). A generalized Yield Locus calculation from texture data, Proc. ICOTOM 7, Noordwijkerhout.

Parniere, P. and Sanz, G. (1976). Appréciation des caractéristiques d'emboutissabilité des tôles minces, Ecole d'été de Métallurgie Physique de Villars-sur-Ollon, Edition du CNRS.

Van Houtte, P. (1987). Calculation of the Yield Locus of Textured Polycrystals Using the Taylor and the Relaxed Taylor Theory, *Textures and Microstructures,* **7,** 29–72.

Van Houtte, P., Mols, K., Van Bael, A. and Aernoudt, E. (1989). Application of yield loci calculated from texture data, *Textures and Microstructures,* **11,** 23–39.

Venkateswara. Rao, K. T. and Ritchie, R. O. (1989). Mechanical properties of Al–Li alloys, *Materials Science and Technology,* 882–895.